Atomic structure of amorphous nanosized silicon powders upon thermal treatment

H. Hofmeister
Max Planck Institute of Microstructure Physics, Weinberg 2, D-06120 Halle, Germany

J. Dutta and H. Hofmann
Powder Technology Laboratory, Department of Materials Science, Swiss Federal Institute of Technology, CH-1015 Lausanne, Switzerland

(Received 29 December 1995)

Amorphous silicon powders prepared by plasma-enhanced chemical vapor deposition, of 8–24-nm-sized particles agglomerated into larger aggregates were annealed in a reducing atmosphere to study the phase transformation behavior of these particles. High-resolution electron microscopy revealed a very rough surface, with structural details of 1 to 2 nm, of the as-prepared single powder particles. Upon 1 h annealing at temperatures between 300 and 600 °C circular contrast features, 1.5–2.5 nm in size, are observed in the amorphous particles, hinting to the formation of a medium-range order. A distinct onset of crystallization is achieved at 700 °C, with structures ranging from very small crystalline ordered regions of 2.5–3.5 nm in size, to fast-grown multiply twinned crystallites. Rapid progress of crystallization, mainly caused by growth twinning, is observed upon annealing at 800 °C. At 900 °C, almost completely crystalline particles are formed. The particles having lattice characteristics of diamond cubic silicon frequently exhibit a faulted structure, because of multiple twinning events. They are covered by an amorphous oxide shell of a 1.5 to 2 nm thickness, which is found to develop with the onset of crystallization. Size and surface roughness of the as-prepared powders are widely preserved throughout all stages of heating, and practically no sintering occurs up to 900 °C. [S0163-1829(96)02728-2]

I. INTRODUCTION

Nanostructured materials are being actively studied in recent times, due to their unique size-dependent properties, which opens up possibilities for new applications.[1–3] Because of the importance in microelectronics fabrication processes, special attention is being paid to studies on silicon powder generation and control in low-pressure silane plasmas.[4] The microstructural properties of such particulates depend on cluster generation processes taking place during powder synthesis.

Electron induced dissociation of silane and subsequent polymerization reactions of negatively charged ions lead to the formation of hydrogenated primary silicon clusters Si_nH_x ($x \sim 1.4 \times n$).[5] Agglomeration of such primary clusters results in the formation of the powder particles.[6] Standard powder characterization techniques, high-resolution electron microscopy (HREM), optical spectroscopy, and Raman and infrared spectroscopy have been utilized to determine the properties of the as-prepared powders.[6–8]

There is some evidence that upon thermal treatment, preformed structures, such as the primary clusters mentioned above, may act as seeds in the crystallization of amorphous semiconductor materials.[8–10] The growth of stable crystallites proceeds by rearranging atoms at the amorphous-to-crystalline interface. Recent work on the crystallization of amorphous semiconductor thin films strongly suggests that lattice defects, such as twins, play an important role in the growth of the crystalline phase.[10–12]

This study is undertaken in the frame of efforts to optimize the synthesis of silicon-based materials for the fabrication of particulates with defined microstructure. This may be achieved by controlling the size, shape, and agglomeration of powder particles during plasma synthesis, followed by the generation of crystalline ordered structures of various extension upon post-deposition thermal treatments. To this aim HREM is well suited for the required structural characterization down to the atomic scale resolution. Here, we will report on the structure and crystallization behavior upon annealing up to 900 °C of amorphous silicon particles studied extensively by HREM. These results will be interesting for understanding the phase transformation behavior in silicon nanoparticles that can also be extended to understand the sintering processes for the preparation of both structural and functional ceramics, as well as for studying confinement effects in silicon nanostructures.[13]

II. POWDER PREPARATION, TREATMENT, AND EXAMINATION

Powders were obtained by the decomposition of silane in a capacitively coupled radio-frequency plasma-enhanced chemical vapor deposition system at room temperature. The processing was carried out with semiconductor pure silane gas at a flow rate of 30 sccm and 0.1-mbar pressure to achieve a low-pressure silane plasma. Further details of the experimental setup have been reported elsewhere.[7]

Thermal treatment of the powders were carried out in a reducing atmosphere to avoid oxidation of the powders in forming gas (92% nitrogen and 8% hydrogen) at various temperatures (300–900 °C) for 1 h or longer periods. Powders exhibiting a reddish-brown to yellowish-orange color that changed to blackish-brown upon annealing, were dispersed by ultrasonic agitation into isopropyl alcohol and then

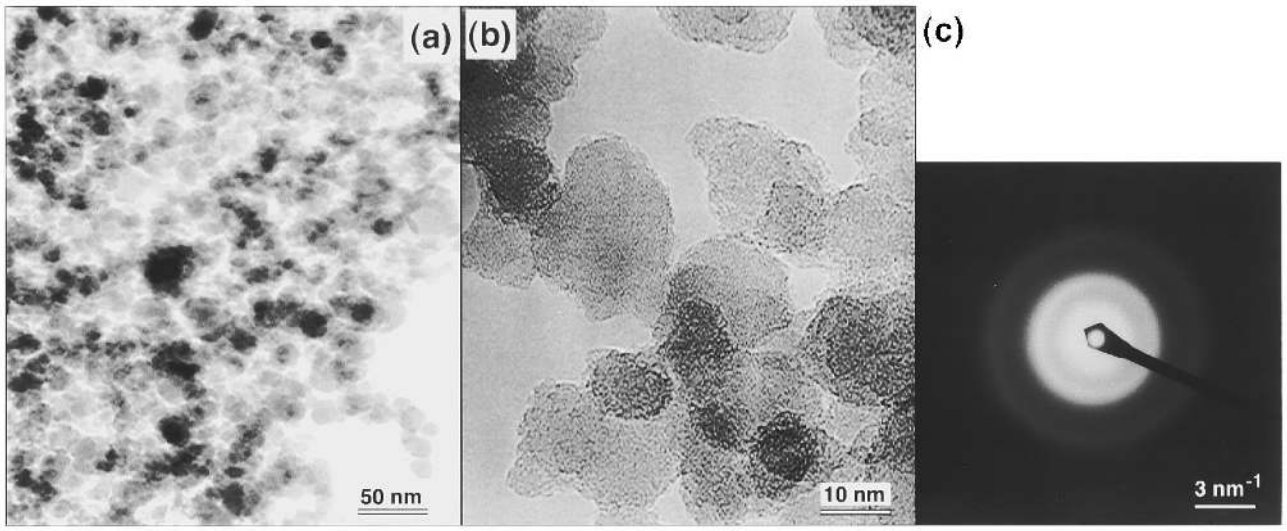

FIG. 1. Conventional electron micrograph (a), corresponding SAED pattern (c), and HREM image (b) of as-prepared powder particles.

transferred to carbon-coated copper grids for electron microscopy inspection. A holey carbon film covering the copper microgrids was used to allow HREM imaging without support disturbance.

Conventional electron microscopy in support of the high-resolution work was done in a JEM 100 C operated at 100 kV. HREM was carried out in a JEM 4000EX operated at 400 kV. Electron micrographs were taken with the objective lens appropriately defocused, so as to achieve optimum contrast (i.e., near Scherzer defocus) of the amorphous particles and to allow imaging of the channels characteristic of the lattice of (110) oriented crystallites as bright dots. With an electron beam current density of less than 10 A cm^{-2} applied during examination, no changes in the observed structures were observed. Real and Fourier space image processing of the micrographs, recorded at 5×10^5 magnification and digitized with an eight bit depth of gray level, by means of the NIH ''Image'' [14] and GATAN ''Digital Micrograph'' programs aimed at noise reduction, contrast enhancement, and reciprocal space characterization.

III. RESULTS AND DISCUSSION

As HREM is well suited to characterize the structural peculiarities of individual powder particles, it needs comparison and a rating in order to extract information on the great many particles forming the powder. The results presented in the following, by observing this demand, are interpreted and discussed in the context of optical, Raman, and infrared spectroscopy results, as well as in the light of the literature on cluster stability and solid phase crystallization of group-IV semiconductor materials.

A. As-prepared powder structure

The as-prepared powder particles are agglomerated in a blackberrylike or cauliflowerlike shape, as shown in a conventional electron micrograph [Fig. 1(a)]. The nearly spherical particles of 8–24 nm in size form a highly porous body of powder having a large specific surface area (~162 m^2 g^{-1}).[6] HREM micrographs as the one shown at low magnification in Fig. 1(b) reveal an amorphous contrast appearance throughout the material. This observation is confirmed by the diffuse rings observed in the selected area electron-diffraction (SAED) pattern, Fig. 1(c), corresponding to the bright-field image of Fig. 1(a). Figure 2 shows two individual amorphous particles having an irregular surface with roughness down to the scale of 1–2 nm. The high surface roughness reflects on the particle formation process by the agglomeration of primary clusters. Typical Raman spectra of the as-prepared powder (phonon band at 507 cm^{-1}) show the optical-phonon band downshifted by approximately 10 cm^{-1}, as compared to bulk crystalline silicon (phonon band at ~520 cm^{-1}).[7] This downshift can be attributed to arise from confinement effects, due to the 2–3 nm-sized clusters, which are observed in the HREM images.

B. Formation of medium-range order

Upon mild annealing for 1 h between 300 to 600 °C, no apparent structural changes were observed. However, careful inspection of the dark-field image revealed nonuniform bright specks, as shown in Fig. 3, which points to a nonhomogeneous atomic distribution. Correspondingly, circular contrast features extending from 1.5 to 2.5 nm in size, as marked by circles in Fig. 4, could be observed in HREM images. Presumably, they are due to partially ordered re-

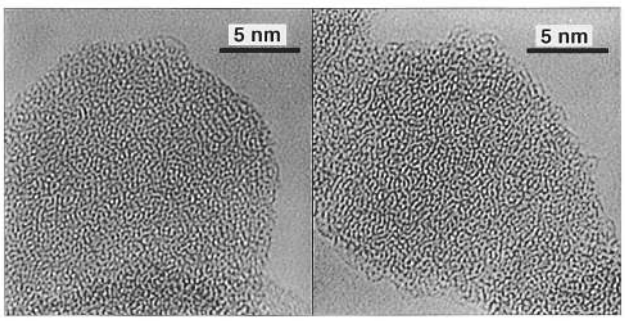

FIG. 2. HREM images of individual amorphous particles of the as-prepared powder.

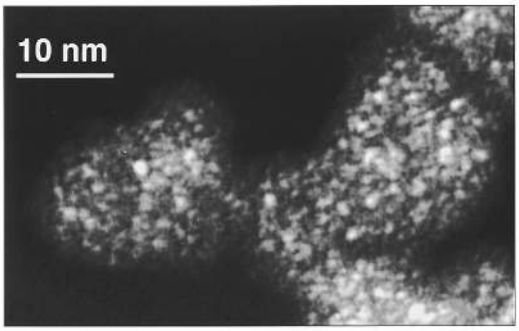

FIG. 3. Dark-field image, recorded by using the intensity of the first diffusive ring [cf. Fig. 1(c)], of the powder after 1-h annealing at 600 °C.

gions, which possibly are present already in the as-prepared powder and become more pronounced upon annealing. Image contrast calculations, according to appropriate structural models, which are under way now,[15] will help to substantiate this observation. Fivefold twinned structures formed upon annealing at higher temperatures suggest the presence of preformed clusters of medium-range order having noncrystallographic symmetry, which serve as seeds in the amorphous-to-crystalline transition. It is obvious to assign these seeds to the primary clusters formed during the particle synthesis process.[5,8]

The stability of clusters of carbon, silicon, and germanium, having a cage or a cage-core configuration, and their possible role in crystallization of the diamond cubic (dc) materials has been discussed in the literature. Hydrogenated carbon clusters C15 and C20, the carbon cage of which corresponds to the hydrocarbon molecules hexacyclopentadecane and dodecahedrane, respectively, are believed to be effective in the formation of diamond from methane.[16] Similarly, a Ge 15 cluster is believed to form the nucleus of fivefold twinned structures in thin-film formation processes by physical vapor deposition.[17] Attachment in a crystallographically favorable position of atoms from the surrounding amorphous phases on the 15 atoms seed, as sketched in perspective view in the upper part of Fig. 5, will lead to a fivefold twinned crystallite, shown in (011) projection with the seed encircled in the lower part. C20, a cluster with

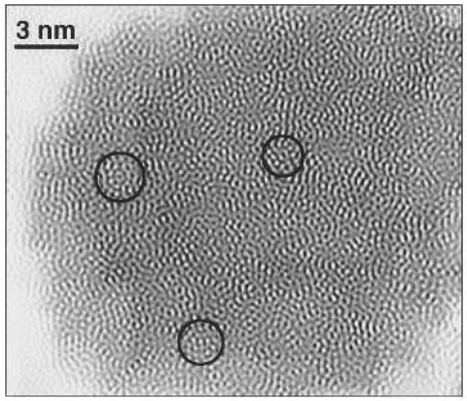

FIG. 4. HREM image of an individual amorphous particle with circular contrast features (some marked by circles) after 1-h annealing at 600 °C.

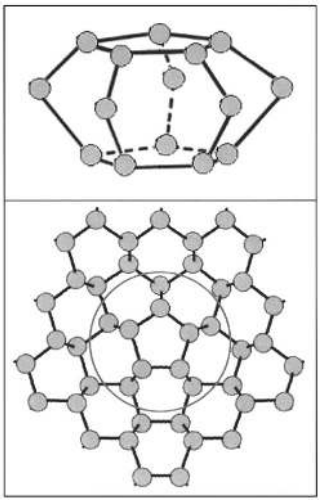

FIG. 5. 15 atoms cluster discussed in Refs. 15 and 16 (upper part), and fivefold twinned dc crystallite nucleated at this seed (lower part).

dodecahedral shape, is found to have the lowest energy as compared with ring or with corannulenelike bowl models.[18] Stability calculations also predict the existence of larger clusters such as Si33, Si39, and Si45, with various cage-core configurations.[19–21] A common feature of all these models is the presence of inherent noncrystallographic symmetries (pentagonal rings) which, because of a possibly enhanced nucleation probability, may play an essential role in the formation of crystalline phases.

C. Onset of crystallization

Prolonged annealing of the powders at 600 °C (5.5 h) results in numerous circular contrast features in HREM images, as shown in Fig. 6. A medium-range order manifests itself to an increasing extent, and with enhanced visibility, even at moderate annealing temperatures. Upon exceeding a critical size, which is estimated to be about 3 nm,[22] stable crystallites may nucleate around these localized ordered ar-

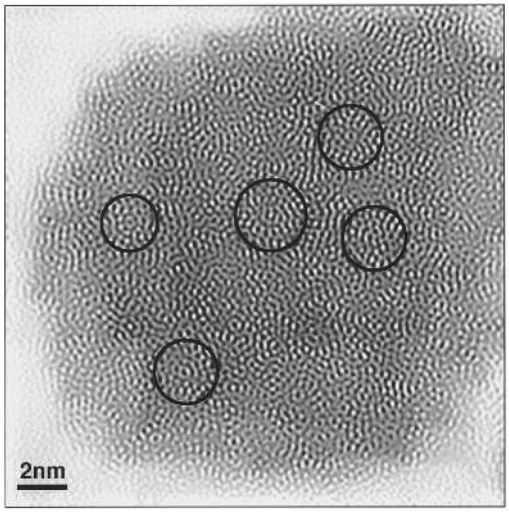

FIG. 6. HREM image of an individual amorphous particle with an increased extent of circular contrast features (see circles) after 5.5-h annealing at 600 °C.

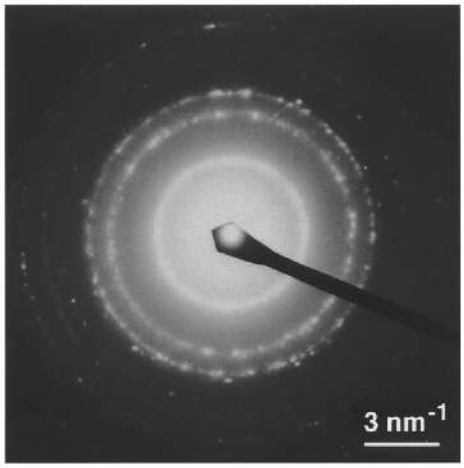

FIG. 7. SAED pattern of the powder after 1-h annealing at 700 °C.

eas where the growth could proceed by rearrangement of atoms at the amorphous-to-crystalline interface. Depending on the crystallographic nature of this interface, there can be a pronounced difference of growth rates in the dc lattice.[23] The portion of {111} faces formed at a growing crystallite will prevail over that of other faces, even for very small sizes, unless there are appropriate defects that enable {111} layer growth.

Upon 1-h annealing at 700 °C, crystallization distinctly sets in. The SAED pattern shown in Fig. 7 exhibits dotted rings superimposed on diffuse broad rings, which is characteristic of a low-dimensional crystalline phase in an amorphous matrix. Frequent events of small-scale crystalline ordering are observed, as shown in Fig. 8, where the diffractogram obtained by fast Fourier transform (FFT) of the image exhibits faint {111} spots. In addition, fast-grown fivefold twinned crystallites occur, an example of which is shown in Fig. 9. The corresponding diffractogram (FFT) clearly exhibits ten spots of a {111}-type of the five mutually twinned units azimuthally rotated to each other by about 72°.

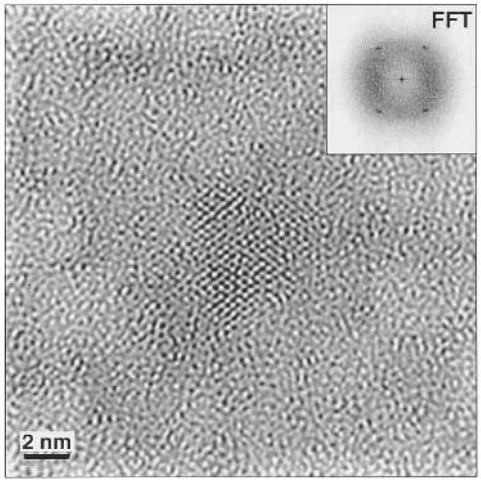

FIG. 8. HREM image of small-scale crystalline ordering in an amorphous particle after 1-h annealing at 700 °C; inset: FFT of the crystalline region.

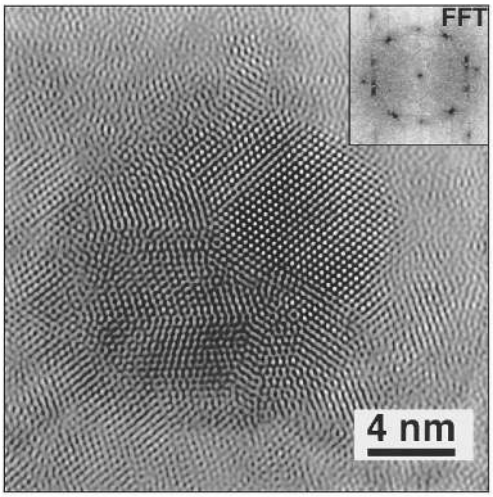

FIG. 9. Fivefold twinned crystallite formed by 1-h annealing at 700 °C with the FFT (inset) exhibiting a pseudopentagonal symmetry.

The nontwinned crystallites are mainly bounded by {111} faces, where further growth is largely restricted.[23] Therefore, they rarely grow to observable sizes as compared to fivefold twinned crystallites, which exhibit rapid growth along the fivefold twin junction, as well as along the twin boundary directions.[24]

Already at this stage of crystallization growth twinning is observed. Since the excess twin energy is rather small, growth twinning, schematically represented in Fig. 10, is very common in dc semiconductor materials.[10–12,16,17,24–26] The growth of stable crystallites proceeds by rearrangement of atoms at the amorphous-to-crystalline $(a-c)$ interface (dashed line). The {111} layer growth requires nucleation of three atoms (shaded), that may be stacked in regular or in twin position, to form a step. Rapid growth is enabled by twinning on {111}, since preferred nucleation sites, requiring rearrangement of only two atoms, are provided at the twin boundary reentrant edges (arrows). The overlay in the center of the scheme represents the HREM image contrast achieved by appropriately defocusing the objective lens to allow imaging of the channels, characteristic of the (110) crystal projection, as bright dots.

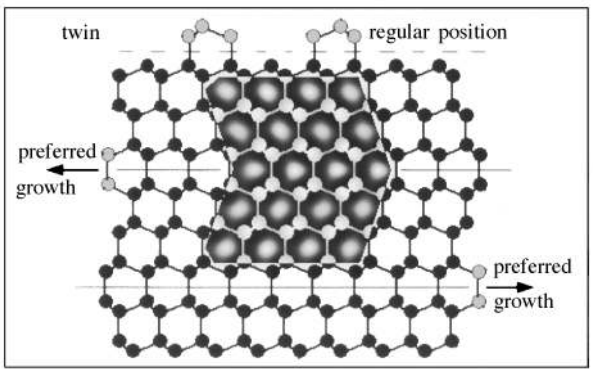

FIG. 10. Schematic representation of the formation and growth of twins in the dc cubic lattice (⟨110⟩ zone axis). Atoms from the amorphous phase (shaded) may be rearranged at a planar $a-c$ interface (dashed line) or at reentrant edges (arrows) of the twin boundaries (solid lines) emerging to the $a-c$ interface.

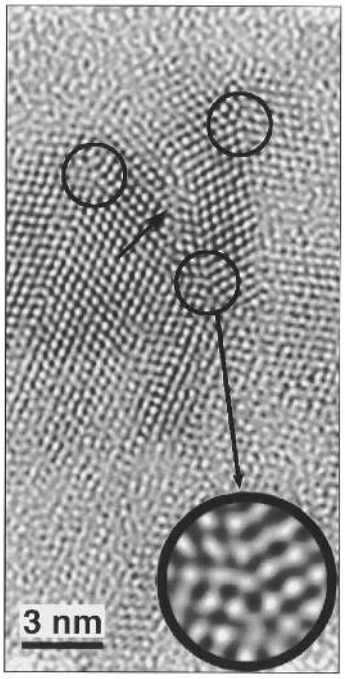

FIG. 11. Fivefold twin junction (circle with arrow) surrounded by parallel and azimuthally rotated twin lamellas with additional multiple twin junctions (encircled) formed by growth twinning.

Typical structures formed by growth twinning are shown in detail in Fig. 11. Repeated twinning on alternate twin planes lead to the formation of parallel and azimuthally rotated twin lamellas and of additional multiple twin junctions (encircled, with the enlarged circle showing the original fivefold twin junction). Because of noncorrelated twinning events higher-order twin boundaries[27] are also formed between twins that lack a simple mirror orientation with respect to {111} faces to adapt lattice misalignments (arrow). By further growth of neighboring units, these sites of inhibited growth become grown-in configurations of higher energy.[12]

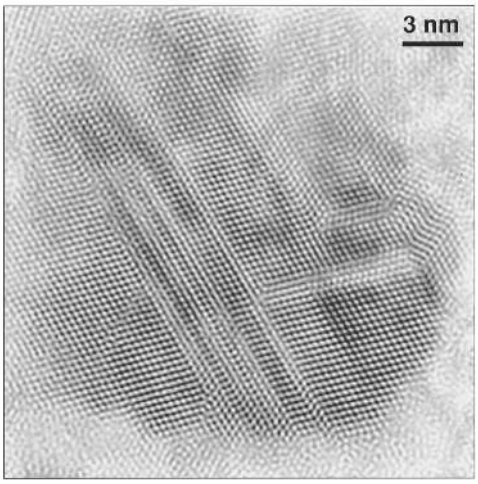

FIG. 12. Heavily twinned structure in a crystallized region after 3.5-h annealing at 800 °C.

D. Progress of crystallization and formation of an oxide surface layer

Raman spectroscopy of the powders indicated increasing crystallinity upon 1-h annealing at 700–900 °C.[7] The downshifted phonon peak of ~507 cm^{-1} sharpens with higher annealing temperature, suggesting an increase in the volume fraction of the crystallites in the material. This peak, downshifted from the Raman peak of crystalline bulk Si at 520 cm^{-1}, suggests a size confined crystalline structural arrangement. A closer insight in the progress of crystallization upon annealing at 800–900 °C is obtained by HREM. In almost all particles, an extended crystal lattice with characteristics of dc Si appears. Because of extensive growth twinning a heavily faulted structure, from which Fig. 12 gives an example, is observed in many particles. Tensile stresses arising from volume contraction during crystallization[28] may be relieved by partial dislocations passing through the lattice thereby creating stacking faults[29] in the two-dimensional twin networks.

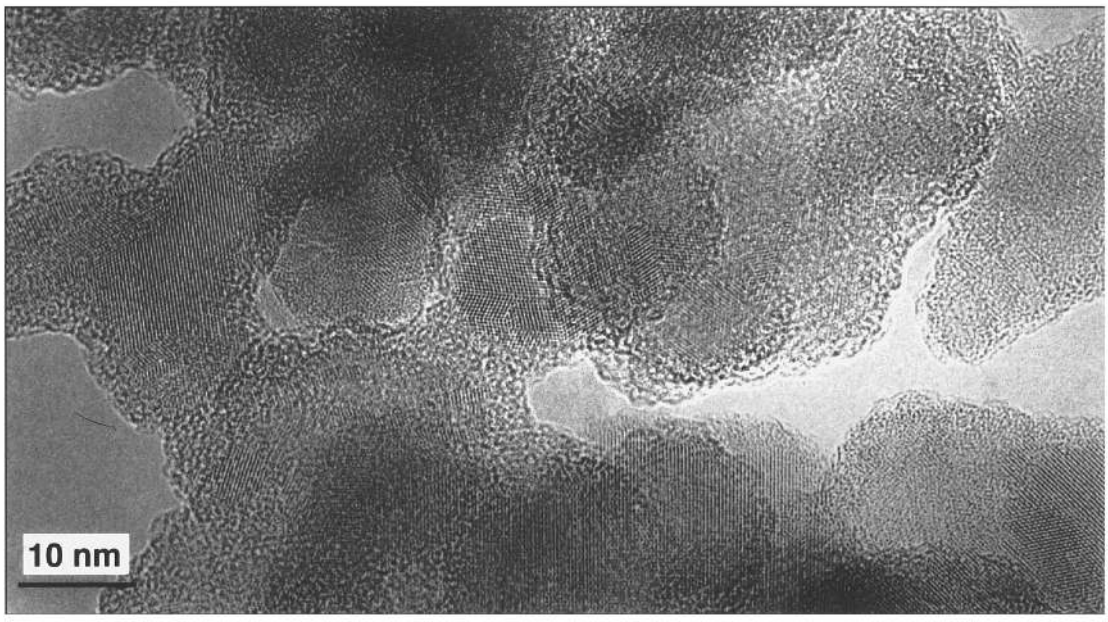

FIG. 13. Overview of the almost completely crystallized powder after 1-h annealing at 900 °C.

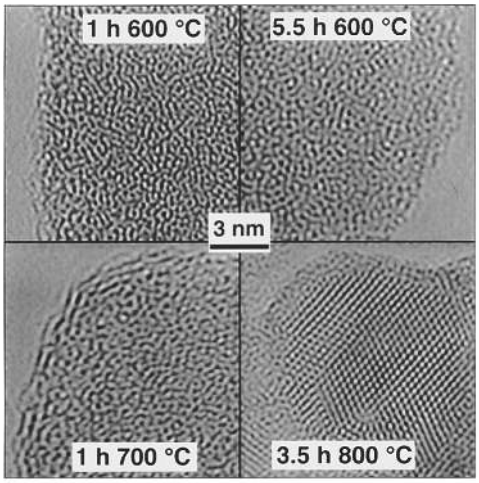

FIG. 14. HREM images of individual powder particles after various stages of annealing, showing different degrees of oxide surface layer formation.

An overview of the powder upon annealing for 1 h at 900 °C is given in Fig. 13. The thermal treatment results in almost completely crystallized particles having a nanocrystalline fabric characterized by a high density of twin boundaries of various order. No considerable change in particle size and the degree of agglomeration was observed. Visualization of the crystal lattice mainly is supported by imaging of {111} lattice plane fringes. Because of the mirror orientation of twinned crystallites first-order twin boundaries are easily recognized. Besides amorphous remnants in the interior of particles, an amorphous shell covering the crystalline cores is distinctly visible.

According to infrared spectroscopy[30] already in the as-prepared powder, a minor quantity of oxygen is present. Rapid formation of silicon oxide, which is presumed to be nonstoichometric, begins with annealing at temperatures of about 350 °C. The formation of an oxide shell was clearly visible by HREM, only in samples annealed at 700 °C or higher, as can be observed by comparison of the images shown in Fig. 14. Oxidation may have taken place, due to the traces of oxygen present in the annealing atmosphere or the rearrangement of the oxygen atoms, which are known to be present in the as prepared powder after exposure to the atmosphere. At 900 °C the oxide surface layer evolves to a thickness of about 2 nm. Because of this oxide layer, sintering of particles is effectively prevented.[31]

IV. CONCLUSIONS

Crystallization of amorphous nanosized silicon powders has been achieved by means of defined annealing procedures. The crystallization is preceded by medium-range order formation, probably with the primary clusters formed during the powder synthesis serving as seeds. Besides small-scale crystalline ordering, from the very beginning of crystallization fast-grown fivefold twinned crystallites occur. The crystallization proceeds mainly by growth twinning, leading to a heavily faulted structure of the dc lattice. During heating surface roughness, particle size and the extent of agglomeration are widely preserved. At 700 °C and above, an amorphous oxide surface layer is formed that effectively prevents sintering of the powder. Crystallization and surface oxide formation, governed by local structural conditions, lead to a variety of structures reflecting the nonhomogeneity of the as-prepared powders. Efforts are in progress now to find out routes for the production of more uniform materials that allow us to obtain particulates with a controlled microstructure.

ACKNOWLEDGMENTS

The authors would like to thank Dr. W. S. Bacsa for Raman spectroscopy. This work has been partially supported by the Fonds National project of the Federal Government of Switzerland under Contract No. 2100-039361.93/1.

[1] L. E. Brus, in *Nanophase Materials: Synthesis-Properties-Applications*, edited by G. C. Hadjipanayis and R. W. Siegel (Kluwer, Dordrecht, 1994), p. 433.
[2] J. L. Dormann, D. Fiorani, and E. Tronc, in *Nanophase Materials: Synthesis-Properties-Applications* (Ref. 1), p. 635.
[3] R. W. Siegel, Nanostructured Mater. **4**, 121 (1994).
[4] G. S. Selwyn, Jpn. J. Appl. Phys. **32**, 3068 (1993).
[5] C. Hollenstein, J.-L. Dorier, J. Dutta, L. Sansonnens, and A. A. Howling, Plasma Sources Sci. Technol. **3**, 278 (1994).
[6] J. Dutta, I. M. Reaney, C. Bossel, R. Houriet, and H. Hofmann, Nanostructured Mater. **6**, 493 (1995).
[7] J. Dutta, W. S. Bacsa, and C. Hollenstein, J. Appl. Phys. **77**, 3729 (1995).
[8] J. Dutta, R. Houriet, Ch. Hollenstein, and H. Hofmann, in *Clusters and Nanostructured Materials*, edited by P. Jena (Nova Science Publishers Inc., New York, 1996).
[9] T. Okabe, Y. Kagawa, and S. Takai, Philos. Mag. Lett. **63**, 233 (1991).
[10] H. Hofmeister and T. Junghanns, J. Non-Cryst. Solids **192/193**, 550 (1995).
[11] J. L. Batstone, Philos. Mag. A **67**, 51 (1993).
[12] H. Hofmeister and T. Junghanns, Trans. Mater. Res. Soc. Jpn. **16B**, 1581 (1994).
[13] S. Schuppler, S. L. Friedmann, M. A. Marcus, D. L. Adler, and Y.-H. Xie, Phys. Rev. B **52**, 4910 (1995).
[14] W. Rasband, 'NIH Image' public domain program, US National Institute of Health, FTP servers, zippy.nimh.nih.gov
[15] H. Hofmeister, J. Dutta, and H. Hofmann, Mater. Sci. Forum (to be published).
[16] S. Matsumoto and Y Matsui, J. Mater. Sci. **18**, 1785 (1983).
[17] T. Okabe Y. Kagawa, and S. Takai, Philos. Mag. Lett. **63**, 233 (1991).
[18] P. R. Taylor E. Bylaska, J. H. Weare, and R. Kawai J. Chem. Phys. Lett. **235**, 558 (1995).
[19] M. V. Ramakrishna and J. Pan, J. Chem. Phys. **101**, 8108 (1994).
[20] J. Pan and M. V. Ramakrishna, Phys. Rev. B **50**, 15 431 (1994).
[21] U. R. Röthlisberger, W. Andreoni, and M. Parinello, Phys. Rev. Lett. **72**, 665 (1994).
[22] S. Veprek, Z. Igbal, and F. A. Sarott, Philos. Mag. B **45**, 137 (1982).

[23] R. Drosd and J. Washburn, J. Appl. Phys. **53**, 397 (1982).
[24] H. Hofmeister and T. Junghanns, Mater. Sci. Forum. **113-115**, 631 (1993).
[25] A. Nakamura, F. Emoto, E. Fujii, A. Yamaoto, Y. Uemoto, K. Senda, and G. Kano, J. Appl. Phys. **66**, 4248 (1989).
[26] W. Luyten, G. van Tendeloo, S. Amelinckx, and J. L. Collins, Philos. Mag. A **66**, 899 (1992).
[27] W. Neumann, H. Hofmeister, and J. Heydenreich, Phys. Status Solidi **146**, 437 (1994).
[28] H. Miura, H. Ohta, and N, Okamoto, Appl. Phys. Lett. **60**, 2746 (1992).
[29] W. Wegscheider, K. Eberl, G. Abstreiter, H. Cerva, and H. Oppolzer, Appl. Phys. Lett. **57**, 1496 (1990).
[30] R. Houriet, J. Dutta, and H. Hofmann, Appl. Surf. Sci. A (to be published).
[31] J. Dutta, H. Hofmann, R. Houriet, H. Hofmeister, and Ch. Hollenstein, Colloids Surf. A (to be published).